Journal of Atmospheric and Solar-Terrestrial Physics 104 (2013) 270–276

Contents lists available at ScienceDirect

Journal of Atmospheric and Solar-Terrestrial Physics

journal homepage: www.elsevier.com/locate/jastp

PMSE observations with the EISCAT VHF- and UHF-radars: Ice particles and their effect on ambient electron densities

Qiang Li [a,*], Markus Rapp [a,b]

[a] Department of Radar Soundings and Sounding Rockets, Leibniz-Institute of Atmospheric Physics at Rostock University, Kühlungsborn, Germany
[b] German Aerospace Center (DLR), Institute of Atmospheric Physics, Oberpfaffenhofen-Wessling, Germany

ARTICLE INFO

Article history:
Received 10 May 2012
Received in revised form
15 October 2012
Accepted 29 October 2012
Available online 14 November 2012

Keywords:
EISCAT
Polar mesosphere summer echoes
Ice particle
Electron density depletions/biteouts

ABSTRACT

It is now well understood that the occurrence of PMSE is closely connected to the presence of ice particles. These ice particles modify the ambient electron density by electron attachment which occasionally leads to large electron density depletions which have also been called 'biteouts'. There has been some debate in the literature regarding the relative depth of such depletions which is usually expressed by the parameter $\Lambda = |Z_A|N_A/n_e$. Here, $|Z_A|N_A$ is the charge number density of ice particles and n_e is the electron density. In this paper, we present, for the first time, the statistical distribution of Λ using measurements with the EISCAT VHF- and UHF-radars. Based on 25 h of simultaneous observations, we derived a total of 757 Λ values based on 15 min of data each. In each of these cases, PMSE were observed with the EISCAT VHF-radar but not with the UHF-radar and the UHF-measurement were hence used to determine the electron density profile. From these 757 cases, there are 699 cases with $\Lambda \ll 1$, and only 33 cases with $\Lambda > 0.5$ (21 cases with $\Lambda > 1$). A correlation analysis of Λ versus PMSE volume reflectivities further reveals that there is no strong dependence between the two parameters. This is in accordance with current PMSE-theory based on turbulence in combination with a large Schmidt-number. The maxima of Λ from each profile show a negative relationship with the undisturbed electron densities deduced at the same altitudes. This reveals that the variability of Λ mainly depends on the variability of the electron densities. In addition, variations of aerosol number densities may also play a role. Although part of the observations were conducted during the HF heating experiments, the so-called overshoot effects did not significantly bias our statistical results. In order to avoid missing biteouts because of a superposition of coherent and incoherent scatter in the UHF-data, we finally calculated spectral parameters n by applying a simple fit to auto-correlation functions as introduced by Strelnikova and Rapp (2010). Corresponding statistical results of the parameter n indicate that charged ice particles do exist in the vicinity of PMSE (i.e., $n < 1$) but they did not efficiently modify ambient electron densities so that clear 'biteouts' are observed.

1. Introduction

The polar mesosphere in summer is host to nanometer-sized ice particles due to the extraordinary thermal structure with mean minimum temperatures down to ~130 K at the mesopause at around 88 km (e.g., Lübken, 1999). Parts of these particles with radii exceeding 20 nm can even be optically observed as noctilucent clouds (or NLC), whereas the whole population of ice particles (in the size range of ~2–100 nm) are supposed to be involved in the creation of strong radar echoes which are termed polar mesosphere summer echoes or PMSE (see e.g., Thomas, 1991; Rapp and Lübken, 2004, for reviews regarding NLC and PMSE, respectively). It is now well confirmed that PMSE and NLC are closely related (e.g., Nussbaumer et al., 1996; von Zahn and Bremer, 1999; Klekociuk et al., 2008). NLC have been long known as direct evidence for ice particles. In contrast, it has only recently been settled that PMSE are created by irregularities in the electron density at the radar Bragg wavelengths (=half the radar wavelength) caused by neutral air turbulence in combination with the effect of charged ice particles (e.g., Kelley et al., 1987; Rapp and Lübken, 2004; Rapp et al., 2008; Nicolls et al., 2009; Li et al., 2010; Varney et al., 2011). Hence, the occurrence of PMSE depends on the ambient electron densities (i.e., there is a lower limit for the occurrence of PMSE, e.g., Rapp et al., 2002, 2009) as well as the presence of charged ice particles which, in turn, are expected to scavenge electrons.

In consequence, it is now understood that charged ice particles also play a crucial role in the charge balance of the polar summer mesopause region where ice particles become negatively charged due to electron attachment and hence effectively scavenge

* Corresponding author. Tel.: +49 3829368144.
E-mail address: liqiang@iap-kborn.de (Q. Li).

1364-6826/$ - see front matter © 2012 Elsevier Ltd. All rights reserved.
http://dx.doi.org/10.1016/j.jastp.2012.10.015

electrons (e.g., Reid, 1990; Jensen and Thomas, 1991; Havnes et al., 1996; Rapp and Lübken, 2001). This process results in electron density depletions or the so-called 'biteouts' (e.g., Ulwick et al., 1988). The occurrence of biteouts is hence considered as strong support for the existence of mesospheric ice particles. So far, electron biteouts in the vicinity of PMSE have routinely been observed with the rocket-borne sensors (e.g., Ulwick et al., 1988; Blix et al., 2003; Rapp et al., 2003; Friedrich et al., 2009, 2011) as well as occasionally with ground-based radars (Röttger et al., 1990; Singer et al., 2011).

As shown in one of the earliest corresponding rocket-borne measurements during the STATE campaign in 1983 (Ulwick et al., 1988) the electron number density may be depleted by as much as a factor of 10 in the presence of PMSE. The question how deep the electron density depletion is in general, however, is still open. While it was originally suspected that Λ-values in excess of ~ 1 were needed for PMSE to occur (Cho et al., 1992), experimental work by Havnes et al. (2011) and Blix et al. (2003) showed that this was generally not the case. Also, Rapp and Lübken (2003) offered a theoretical explanation for this apparent discrepancy between theory and observations (see their Appendix B). Blix et al. (2003) carried out a statistical study of the correlation between Λ and PMSE profiles based on four sounding rocket flights and derived a distribution of Λ in the presence of PMSE. They showed that only in 15% of all altitude bins Λ exceeded a value of 1 whereas in $\sim 75\%$ of all altitude bins Λ was even less than 0.5 (see their Table 4 for details). Unfortunately, measurements of four rocket flights must still be considered as poor statistics and they also suffer from the constraint that there is a big difference in the observing volumes between radars and sounding rockets. In this study, it is our aim to derive a statistically reliable distribution of Λ from the measurements of electron densities with the EISCAT UHF-radar in the presence of PMSE simultaneously observed with the collocated EISCAT VHF-radar. Furthermore, we present the correlation between Λ and the volume reflectivities of the VHF-PMSE. The structure of this paper is as follows: In Section 2, we describe the experimental details as well as the data base for the current analysis. Next, we present a new method to estimate Λ from the radar observations in Section 3 where we also present the statistical results of the derived Λ-values. In order to avoid missing electron biteouts because of a superposition of coherent and incoherent scatter in the UHF-data, we further check the spectral shapes based on the analysis of the auto-correlation functions (Section 4). Our final conclusions and proposals for future research are presented in Section 5.

2. Experimental details

The measurements analyzed in this paper were performed in the summer seasons from 2003 to 2007 with the EISCAT VHF- and UHF-radars which are collocated at Ramfjordmoen near Tromsø, Norway (69.6 °N,19.2 °E). Detailed descriptions of these two radars can be found in Baron (1986) and Folkestad et al. (1983), respectively. In order to deal with a homogeneous dataset, all corresponding observations with both radars were simultaneously conducted using the so-called 'arcdlayer'-experiment or its special version, i.e., the 'arcdlayer-ht'-experiment. The latter was applied during heating experiments with the RF heating facility of the EISCAT Tromsø radar site (Rietveld et al., 1993; Naesheim et al., 2008). See also Li and Rapp (2011) for a detailed description of the experiments and datasets including a detailed list with corresponding technical parameters. In the current analysis, the heating parts of the observations are not considered and are removed before integration of the data was carried out.

Table 1
Observations with the EISCAT VHF- and UHF-radars analyzed in this paper.

Date	Time [UT]	Experiment	UHF-PMSE
2003-06-30	08:00–10:00	arcdlayer	Yes
2003-07-01	08:00–11:00	arcdlayer	No
2003-07-02	07:00–10:00	arcdlayer	No
2004-07-07	07:00–08:00	arcdlayer_ht	No
2004-07-14	07:00–10:00	arcdlayer_ht	Yes
2005-07-04	08:00–13:00	arcdlayer_ht	Yes
2005-07-05	11:00–13:00	arcdlayer_ht	Yes
2005-07-10	07:00–08:00	arcdlayer_ht	No
2007-08-11	08:00–10:00	arcdlayer	No
2007-08-12	10:00–13:00	arcdlayer	No

The EISCAT VHF- and UHF-radars are both incoherent scatter (IS) radars which are a powerful tool for studying the Earth's ionosphere. In the D-region (i.e, at altitudes below ~ 95 km) the received echoes are mainly due to scattering from electron density fluctuations dominated by highly damped ion acoustic waves (e.g., Dougherty and Farley, 1963; Tanenbaum, 1968; Mathews, 1978). The total echo power depends on the number density of electrons and can hence be used to estimate the electron number density. In the presence of PMSE, the measurements with the EISCAT VHF and UHF-radars are a superposition of coherent scatter from PMSE and incoherent scatter from the ambient plasma at mesospheric altitudes. Due to the well-known frequency dependence of PMSE, the VHF-radar observes PMSE much more frequently than the UHF-radar (e.g., Li and Rapp, 2011). However, given a sufficiently large electron density (in our case determined by the detection limit of the UHF-radar of about $\sim 1 \times 10^9$ m^{-3}, see e.g., Friedrich and Kirkwood, 2000), the UHF observations may be dominated by incoherent scatter from the D-region electrons such that they can be used to infer electron densities in the presence of PMSE observed with the VHF-radar. A list of the corresponding observations analyzed in this study is presented in Table 1.

The original data-dump provided by the EISCAT-experiments described above are auto-correlation functions (ACF, i.e., the Fourier transform of the Doppler spectrum according to the Wiener–Khinchine theorem) which consist of 127 lags with 1.35 ms resolution for 'arcdlayer'-experiment and with 1.562 ms resolution for 'arcdlayer-ht'-experiment. Using the well documented 'GUISDAP' software package (Lehtinen and Huuskonen, 1996), the observations are routinely analyzed off-line in terms of electron number densities (or 'apparent' electron densities for the case of PMSE). Such derived 'apparent' electron number densities can be converted to volume reflectivities using the well-known relation

$$\eta = \sigma \times N_e \tag{1}$$

where $\sigma = 5 \times 10^{-29}$ m^2 is half the scattering cross section σ_e of an electron ($\sigma = \sigma_e \times (1 + T_e/T_i)^{-1} = \sigma_e/2$) and N_e is the 'apparent' electron number density (e.g., Röttger and LaHoz, 1990). Note that the term 'apparent' electron density is meant to express that the signal is not a measure of real electron density but due to coherent scatter of PMSE which adds to the incoherent scatter (and usually outperforms the latter during strong VHF-PMSE by far).

3. Method to derive Λ and statistical results

Fig. 1 sketches a typical altitude profile of electron densities (undisturbed electron density in dashed line and observed electron density in solid line) in a "biteout" situation. From charge

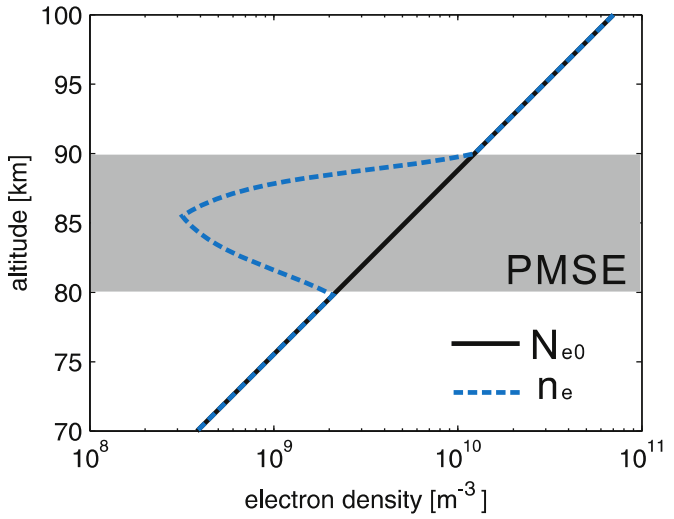

Fig. 1. Schematic picture of typical altitude profiles of undisturbed electron density N_{e0} (solid line) and observed electron density n_e (dashed line) in a 'biteout' situation. The shaded area indicates the altitudes where PMSE occur.

neutrality, we may assume $n_e = N_{e0} - N_A|Z_A|$, where N_{e0} is the undisturbed electron density in the absence of ice particles. Note that this assumption implies that the positive ion density disturbance due to the presence of aerosol particles is small compared to their effect on electrons. Indeed, this assumption is usually valid except under conditions of very deep biteouts (see Rapp and Lübken, 2001, their Fig. 1 and the corresponding discussion).

The ratio between charge number density of ice particles and electron number density can then be determined by

$$\Lambda = |Z_A|N_A/n_e = (N_{e0} - n_e)/n_e \quad (2)$$

where N_{e0} must be determined from the measured electron density profile by interpolation between below and above the depletion layer.

Fig. 2 presents three typical cases out of all the observations. The gray lines in each panel show fifteen 1-min electron density profiles deduced from the UHF observations with their mean profile as a blue line (i.e., n_e, see bottom abscissa). In order to derive the undisturbed electron density, we fitted the mean profiles excluding the altitude ranges of the UHF-PMSE signals and the electron biteouts by an eighth order polynomial. The fitting lines are shown as black dashed lines (i.e., N_{e0}). Based on Eq. (2), Λ-values were calculated and are shown as red lines with dots (see middle abscissa). For comparison, the profiles of PMSE volume reflectivities simultaneously observed with the EISCAT VHF-radar are also overplotted as green lines (see top abscissa).

We have next applied this analysis to all the observations. From 25 h of simultaneous observations, we derived 757 Λ-values from the UHF observations in the presence of VHF-PMSE. The lower panel of Fig. 3 presents the distribution of the derived Λ-values. For the large majority of cases (699 cases), the Λ values are within the range from -0.3 to 0.3 which can be considered close to 0 and hence no strong electron biteouts are observed. Please note that the occurrence of negative Λ-values simply reveals the imperfection of our algorithm to determine the undisturbed electron density and may hence be considered as a systematic error of our analysis. This means that the quoted Λ-values should be considered to have error bars of $\pm$ 0.3 because of this effect. Nevertheless, this method still allows to quantify depletions with Λ-values larger than say 0.5. From 757 cases, there are only 33 cases with $\Lambda > 0.5$ marked with red crosses in

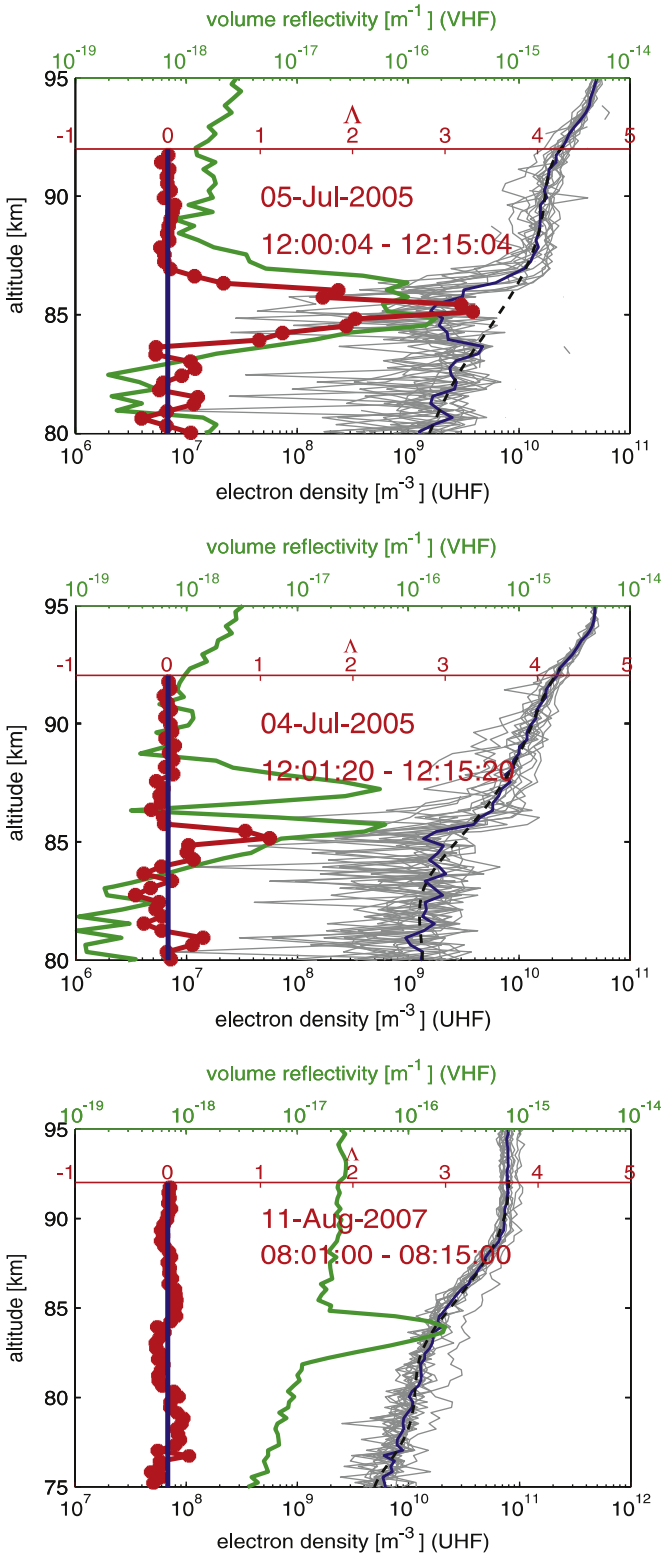

Fig. 2. Samples of electron biteouts: strong depletion, moderate depletion, no depletion in the upper, middle, and lower panels, respectively.

the upper panel (21 cases with $\Lambda > 1$), i.e., only 4.4% of all the observations.

In addition, the upper panel of Fig. 3 reveals that the distribution of Λ-values versus the volume reflectivities of VHF-PMSE shows no obvious correlation between them. This is, however, expected: according to the turbulence with large Schmidt number

theory (TWLS-theory) of PMSE, the volume reflectivity of PMSE is most strongly controlled by the Schmidt number which can change the volume reflectivity at given wavenumber k by many orders of magnitude whereas the dependence on Λ is much less pronounced (e.g., Rapp and Lübken, 2003; Varney et al., 2011).

The distribution of the Λ-values shows variability within a large range and strong biteouts are very rare. In a biteout situation, aerosol particles capture the ambient electrons resulting in depletion in the remaining free electron densities. In the left panel of Fig. 4, we sketch typical altitude profiles of charged aerosol particles (dashed line) and electrons (dotted and solid lines) for low densities (a) and high densities (b), respectively. In assumption of a constant mount of aerosol particles (hence the mount of electrons they can capture is constant), low electron densities are supposed to lead to deep biteouts and vice versa. In order to investigate the conditions for a strong biteout and the reason for the variability of Λ, we perform an analysis of the relationship between the maxima of Λ and the estimated undisturbed electron densities N_{e0} at the same altitudes. The results reveal that there is a negative relationship between the two parameters with a significance to a level of more than 99.9% (see right panel of Fig. 4). These results provide a strong support that the variability of Λ mainly depends on the variability of electron densities. Note, the variability of Λ also, of course, depends on the variability of number density of aerosol particles (see Eq. (2)) which, however, is much smaller compared to the variability of electron number densities.

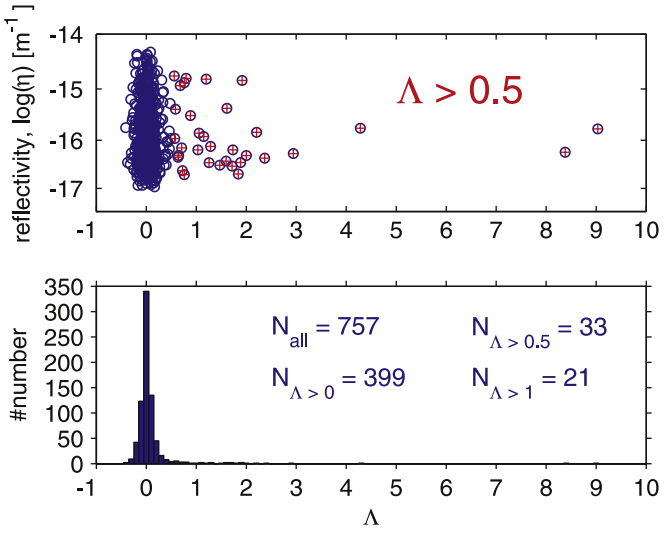

Fig. 3. Upper panel: scatter plot of the derived Λ values from the UHF observations against the corresponding volume reflectivities of the VHF-PMSE (Λ with values larger than 0.5 are marked with red crosses). Lower panel: histogram of Λ with the number of Λ in the different ranges indicated in the insert. (For interpretation of the references to color in this figure caption, the reader is referred to the web version of this article.)

4. Discussion

Before we may draw final conclusions on the statistical distribution of Λ, a number of caveats need to be considered.

In the current study, part of the observations were conducted during the HF heating experiments (Rietveld et al., 1993). In order to investigate if the so-called overshoot effects in the PMSE modulation experiments have influence on our statistical results. We replotted the distribution of Λ from the observations after removing the part with heater on as well as the part presumably disturbed by the overshoot effects (not shown here). In this study, the heating experiments were conducted with heater 20 s on and 160 s off and the overshoot effects are assumed to last for 40∼60 s (e.g., Kassa et al., 2005). Hence the heating parts and the parts with overshoot effects (of 60 s since the heater on) were removed and the remaining observations were integrated over 15 min intervals. This results in 30 cases with $\Lambda > 1$ from 627 cases in total, i.e., there is no significant difference after this exercise and the conclusions are the same with before.

In addition, we must be very careful when judging the cases showing no biteouts only based on the electron density profiles. This is because the UHF observations could be a superposition of incoherent scatter from the disturbed electron densities and coherent scatter from the UHF-PMSE which, however, does not stand well out of the ambient incoherent scatter from the ionospheric plasma (see Figure 1 in Strelnikova and Rapp, 2010, and corresponding discussion). This scenario is illustrated in Fig. 5. An electron biteout does exist but it cannot be detected because it is masked by the presence of a weak UHF-PMSE signal resulting in an overall apparently smooth electron density profile. It has been recently shown that the presence of nanometer-size ice particles leads to a significant change of the observed spectral shape compared to theoretical results according to classical ISR theory

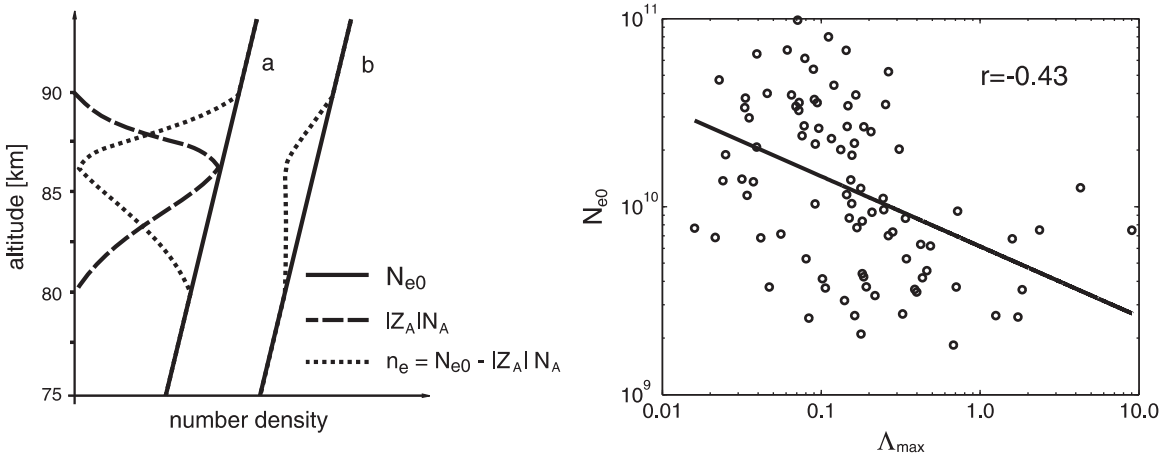

Fig. 4. Left panel: schematic picture of typical altitude profiles of electrons and charged aerosol particles in a 'biteout' situation for low electron densities (a) and high electron densities (b), respectively. Right panel: scatter plot of Λ_{max} from each profile (see red line in Fig. 2) versus N_{e0} derived at the same altitudes. A regression line is indicated with solid line. In addition, the correlation coefficient is indicated in the insert which is highly significant (i.e., above the 99.9% level). (For interpretation of the references to color in this figure caption, the reader is referred to the web version of this article.)

(Cho et al., 1998; Rapp et al., 2007; Strelnikova et al., 2007). In this section, we check the corresponding spectral shapes in order to find out whether such cases of superposition do frequently occur and create a bias in our data.

Following Strelnikova and Rapp (2010), there are three types of spectra (or ACFs) for ISR-observations from the D-region, i.e., Gaussian, Lorentzian, and a superposition of two Lorentzians. These three types correspond to coherent scatter like PMSE signals, incoherent scatter, and incoherent scatter modified by the presence of charged heavy particles, respectively. The third type occurs due to the Coulomb coupling between electrons and positive ions as well as between electrons and charged ice particles, respectively (see Cho et al., 1998, for details). In this section, our task is to clarify whether the UHF observations without detectable electron biteouts in the presence of VHF-PMSE are due to incoherent scatter under the influence of charged ice particles or due to the coherent scatter from the UHF-PMSE, or a mixture of both. We hence apply the same analysis technique developed by Strelnikova and Rapp (2010) who employed a simple robust technique to quantify the spectral shape by fitting the magnitudes of the corresponding auto-correlation functions (ACF). The expression of the ACF magnitude is approximated as (Jackel, 2000; Moorcroft, 2004)

$$ACF(\tau) = ACF_{\tau=0} \cdot \exp\{-(\tau/\tau_e)^n\} \quad (3)$$

where ACF is the magnitude of auto-correlation function, τ is the lag time at which the ACF is evaluated, τ_e is the decay time (which is inversely related to the spectral width), and n is an exponent describing the shape of the spectrum. That is, $n=1$ and $n=2$ represent a Lorentzian (=pure incoherent scatter) and a Gaussian (=coherent scatter), respectively, whereas $n<1$ marks the cases with the presence of charged ice particles (Rapp et al., 2007; Strelnikova and Rapp, 2010).

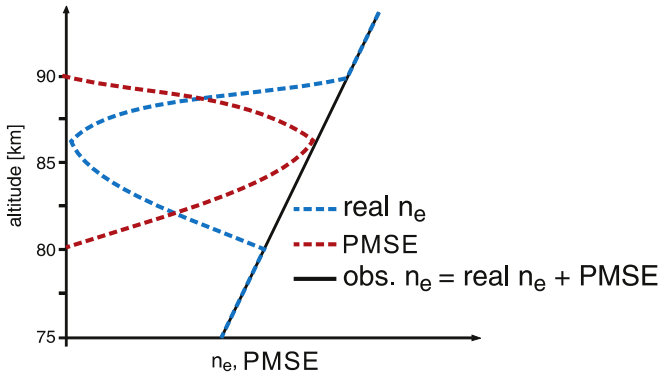

Fig. 5. Schematic picture of a scenario where an electron biteout exists but is not detected because it is covered by UHF-PMSE. The observed profile and the real electron densities are indicated in black and blue, respectively. The UHF-PMSE signal is indicated in red. (For interpretation of the references to color in this figure caption, the reader is referred to the web version of this article.)

According to the above, there should be two possibilities for the spectral shapes derived from the simultaneous observations with both radars when the VHF-radar observed pronounced PMSE and the UHF observations show an apparently undisturbed electron density profile, i.e., the parameter n should be close to 2 for the VHF observations whereas it should either also be close to 2 for the cases in the presence of UHF-PMSE or smaller than 1 in the presence of charged ice particles (and pure incoherent scatter). A typical example is shown in Fig. 6 (see the left panel of Fig. 7 for evidence that there is pronounced VHF-PMSE and an apparently smooth profile of electron densities in the UHF observations). The original data are shown in red crosses. We then fitted them with Eq. (3) (black) as well as under the assumption of a Gaussian shape ($n=2$ in Eq. (3), green) and a Lorentzian shape ($n=1$, blue), respectively. The derived parameters n are indicated in the insert. For the UHF observations, the ACF obviously cannot be described neither by a Lorentzian spectral shape nor a Gaussian spectral shape. In the case of the VHF observations the ACF approximately reveals a Gaussian shape with $n=1.62$ indicative of coherent scatter from PMSE. In contrast, the UHF data yield a best fit of $n=0.38$ corresponding to incoherent scatter under the influence of the charged ice particles. As a next step, Fig. 7 shows the results of a corresponding analysis for observations obtained on 11 August 2007 (08:35–09:00 UT). Indeed, n is found to be close to a value of 2 for altitudes where the VHF-radar detects a PMSE and it is close to 1 (and indicative of incoherent scatter) at altitudes above and below. In contrast, the UHF-data show n-values close to 1 below the PMSE-layer but then change to values less than 1 within and above the layer.

Finally, this analysis was applied to all the measurements listed in Table 1. The corresponding results of the derived

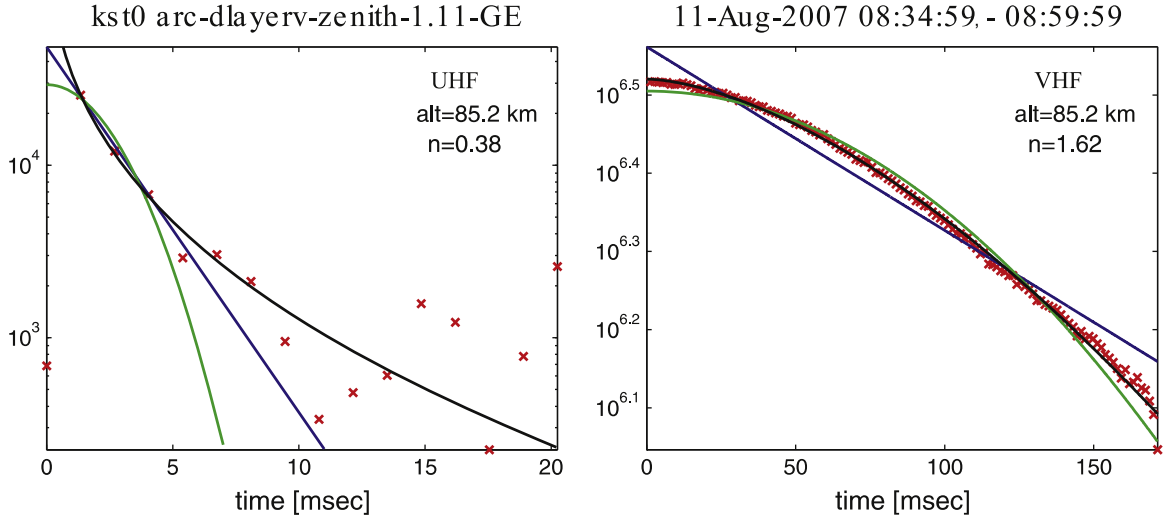

Fig. 6. Examples of ACFs obtained from the observations with the EISCAT UHF (left panel) and VHF (right panel) radars. The magnitudes of the ACFs were fitted with Eq. (3) (black) as well as with the assumption of a Gaussian spectral shape (green) and a Lorentzian spectral shape (blue). The ACF-analysis results in $n<1$ for the UHF observations (modified incoherent scatter by the presence of charged ice particles) and n close to 2 for the VHF observations (coherent scatter from the PMSE signals). (For interpretation of the references to color in this figure caption, the reader is referred to the web version of this article.)

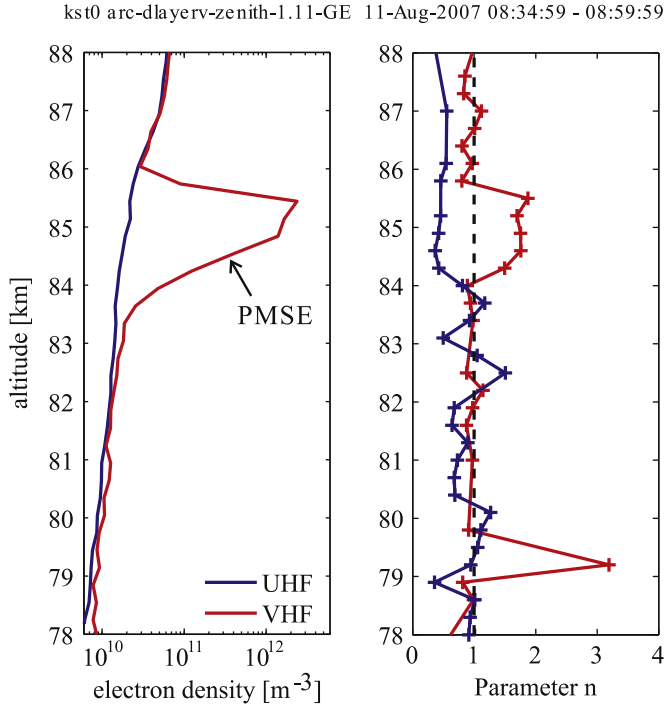

Fig. 7. Left panel: example of a comparison between the profiles of electron densities deduced from the VHF- and UHF-observations (in red and blue, respectively). Right panel: same as the left panel, but for the profiles of the derived parameter *n*. (For interpretation of the references to color in this figure caption, the reader is referred to the web version of this article.)

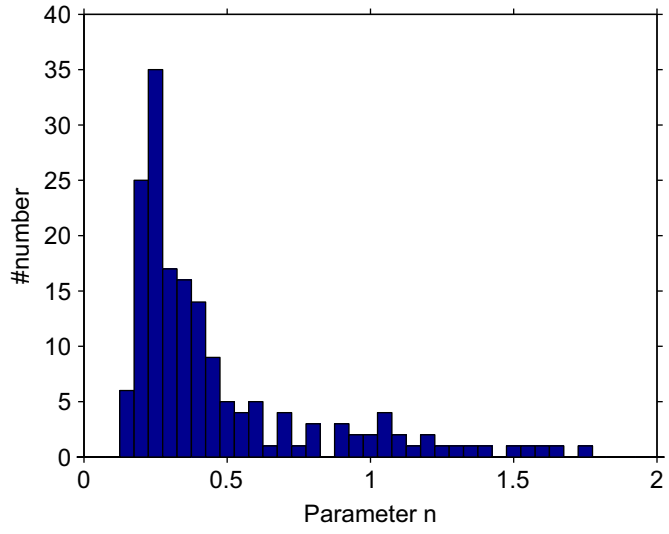

Fig. 8. Distribution of parameter *n* derived from the UHF-observations in the presence of PMSE observed with the EISCAT VHF-radar. For large majority of cases, $n<1$ indicative of the presence of charged ice particles and no UHF-PMSE.

parameters *n* (for UHF-observations at altitudes with VHF-PMSE) are shown in Fig. 8. The parameter *n* shows the large majority of cases with values smaller than 1, which indicates that there are charged ice particles present in the vicinity of VHF-PMSE but no PMSE were observed with the EISCAT UHF-radar.

Coming back to the statistics of Λ-values presented in the previous section we conclude that this statistics is not biased by an un-identified superposition of coherent and incoherent scatter. In all, we can conclude that the distribution shown in Fig. 3 nicely confirms the previous results of Blix et al. (2003), albeit on the basis of a much improved statistics.

5. Conclusions

In this paper, we have presented the statistical distribution of Λ, i.e., the ratio between charge number density of ice particle ($|Z_A|N_A$) and electron density (n_e), based on the analysis of 25 h observations with the EISCAT UHF-radars in the presence of PMSE simultaneously observed with the EISCAT VHF-radar. From a total of 757 cases, there are 699 cases with $\Lambda \ll 1$ and only 33 cases with $\Lambda > 0.5 \pm 0.3$ (21 cases with $\Lambda > 1 \pm 0.3$). The results derived from our radar observations show an overall consistency with the previous (but much more sporadic) in situ measurements (Havnes et al., 2011; Blix et al., 2003; Rapp et al., 2003). With the calibrated observations of IS radars, we also presented the distribution of Λ versus PMSE volume reflectivities of VHF-PMSE and found that there is no close relation between these two parameters which is in agreement with theoretical expectations (e.g., Rapp and Lübken, 2003; Varney et al., 2011). We further presented a negative relationship between Λ_{max} and the corresponding N_{e0} at the same altitudes and hence conclude that the variability of Λ mainly depends on the variability of electron densities.

In addition, we redid the whole analysis after removing the part with heater on and the part with the so-called overshoot effects and did not find significant difference from before. We further investigated whether the absence of frequent electron biteouts in the UHF-data could have been possibly due to a superposition of incoherent and coherent scatter hence masking the presence of an electron depletion. For this purpose, we investigated corresponding spectral shapes based on an ACF-analysis with one simple fitting parameter, i.e., the parameter *n*. This parameter obtains a value of 1 for a Lorentzian spectral shape of the ACF indicative of pure incoherent scatter from the collision-dominated D-region, a value of 2 for a Gaussian spectral shape indicative of coherent scatter like PMSE, and a value of smaller than 1 for incoherent scatter under the influence of the charged ice particles. Applying this fitting procedure to all data reveals that the large majority of UHF-observations is characterized by $n<1$ ($\sim 88.2\%$) in the presence of VHF-PMSE. This finding confirms that the distribution of Λ-values is not biased by a superposition of coherent and incoherent scatter. In addition, this result underlines the importance of the presence of charged ice particles for the generation of PMSE and demonstrates that small relative concentrations of charged ice particles are sufficient to create these very strong coherent echoes.

For the future, the EISCAT observations should be combined with independent electron density observations making use of the Faraday rotation and absorption effect in the mid-frequency range (e.g., Singer et al., 2011). This would push the lower limit of detectable electron densities and allow insight into ionization conditions which are not accessible with the EISCAT radars.

Acknowledgments

The project was supported by DFG in the frame of the CAWSES priority program under Grants RA 1400/2-1, RA 1400/2-2, and RA 1400/2-3. We greatly acknowledge very helpful discussions with I. Strelnikova including the provision of a software package for spectral characterization. EISCAT is an international association supported by research organization in China (CRIRP), Finland (SA), France (CNRS, till end 2006), Germany (DFG, formerly MPG),

Japan (NIPR and STEL), Norway (NFR), Sweden (VR), and the United Kingdom (PPARC).

References

Baron, M., 1986. EISCAT progress 1983–1985. Journal of Atmospheric and Terrestrial Physics 48, 767–772.

Blix, T.A., Rapp, M., Lübken, F.-J., 2003. Relations between small scale electron number density fluctuations, radar backscatter and charged aerosol particles. Journal of Geophysical Research 108 (D8), 8450, http://dx.doi.org/10.1029/2002JD002430.

Cho, J.Y.N., Hall, T.M., Kelley, M.C., 1992. On the role of charged aerosols in polar mesosphere summer echoes. Journal of Geophysical Research 97, 875–886.

Cho, J.Y.N., Sulzer, M.P., Kelley, M.C., 1998. Meteoric dust effects on D-region incoherent scatter radar spectra. Journal of Atmospheric and Terrestrial Physics 60, 349–357.

Dougherty, J.P., Farley, D.T., 1963. A theory of incoherent scattering of radio waves by a plasma: 3. Scattering in a partly ionized gas. Journal of Geophysical Research 68, 5473–5486.

Folkestad, K.T., Hagfors, T., Westerlund, S., 1983. EISCAT: an updated description of technical characteristics and operational capabilities. Radio Sciences 18, 867–879.

Friedrich, M., Torkar, K.M., Singer, W., Strelnikova, I., Rapp, M., Robertson, S., 2009. Signatures of mesospheric particles in ionospheric data. Annales Geophysicae 27, 823–827.

Friedrich, M., Kirkwood, S., 2000. The D-region background at high latitudes. Advances in Space Research 25 (1), 15–23.

Friedrich, M., Rapp, M., Plane, J., Torkar, K.M., 2011. Bite-outs and other depletion of mesospheric electrons. Journal of Atmospheric and Terrestrial Physics 73, 2201–2211.

Havnes, O., Trøim, J., Blix, T., Mortensen, W., Næsheim, L.I., Thrane, E., Tønnesen, T., 1996. First detection of charged dust particles in the Earth's mesosphere. Journal of Geophysical Research 101, 10839–10847.

Havnes, O., Brattli, A., Aslaksen, T., Singer, W., Blix, T., Thrane, E., Trøim, J., 2011. First common volume observations of layered plasma structures and polar mesospheric summer echoes by rocket and radar. Geophysical Research Letters 28, 1419–1422.

Jackel, B.J., 2000. Characterization of auroral radar power spectra and autocorrelation functions. Radio Science 35, 1009–1024.

Jensen, E., Thomas, G.E., 1991. Charging of mesospheric particles: implications of electron density and particle coagulation. Journal of Geophysical Research 96, 18,603–18,615.

Kassa, M., Havnes, O., Belova, E., 2005. The effect of electron bite-outs on artificial electron heating and the PMSE overshoot. Annales Geophysicae 23, 3633–3643.

Kelley, M.C., Farley, D.T., Röttger, J., 1987. The effect of cluster ions on anomalous VHF backscatter from the summer polar mesosphere. Geophysical Research Letters 14, 1031–1034.

Klekociuk, A.R., Morris, R.J., Innis, J.L., 2008. First southern hemisphere common volume measurements of pmc and pmse. Geophysical Research Letters 35, L24804.

Lehtinen, M.S., Huuskonen, A., 1996. General incoherent scatter analysis and GUISDAP. Journal of Atmospheric and Terrestrial Physics 58, 435–452.

Li, Q., Rapp, M., 2011. PMSE-observations with the EISCAT VHF and UHF-radars: statistical properties. Journal of Atmospheric and Solar-Terrestrial Physics 73 (9), 944–956, http://dx.doi.org/10.1016/j.jastp.2010.05.015.

Li, Q., Rapp, M., Röttger, J., Latteck, R., Zecha, M., Strelnikova, I., Baumgarten, G., Hervig, M., Hall, C., Tsutsumi, M., 2010. Microphysical parameters of mesospheric ice clouds derived from calibrated observations of polar mesosphere summer echoes at Bragg wavelengths of 28 m and 30 cm. Journal of Geophysical Research 115, D00I13, http://dx.doi.org/10.1029/2009JD012271.

Lübken, F.-J., 1999. Thermal structure of the Arctic summer mesosphere. Journal of Geophysical Research 104, 9135–9149.

Mathews, J.D., 1978. The effect of negative ions on collision-dominated Thomson scattering. Journal of Geophysical Research 83, 505–512.

Moorcroft, D.R., 2004. The shape of auroral backscatter spectra. Geophysical Research Letters 31(9).

Naesheim, L.I., Havnes, O., Hoz, C.L., 2008. A comparison of polar mesosphere summer echo at VHF (224 MHz) and UHF (930 MHz) and the effects of artificial electron heating. Journal of Geophysical Research 113.

Nicolls, M.J., Kelley, M.C., Varney, R.H., Heinselman, C.J., 2009. Spectral observations of polar mesospheric summer echoes at 33 cm (450 MHz) with the Poker Flat incoherent scatter radar. Journal of Atmospheric and Solar-Terrestrial Physics 71, 662–674.

Nussbaumer, V., Fricke, K.-H., Langer, M., Singer, W., von Zahn, U., 1996. First simultaneous and common-volume observations of NLC and PMSE by lidar and radar. Journal of Geophysical Research 101, 19161–19167.

Rapp, M., Lübken, F.-J., 2001. Modelling of particle charging in the polar summer mesosphere: Part 1—general results. Journal of Atmospheric and Solar-Terrestrial Physics 63, 759–770.

Rapp, M., Gumbel, J., Lübken, F.-J., Latteck, R., 2002. D-region electron number density limits for the existence of polar mesosphere summer echoes. Journal of Geophysical Research 107 (D14) http://dx.doi.org/10.1029/2001JD001323.

Rapp, M., Lübken, F.-J., 2003. On the nature of PMSE: electron diffusion in the vicinity of charged particles revisited. Journal of Geophysical Research 108 (D8), 8437, http://dx.doi.org/10.1029/2002JD002857.

Rapp, M., Lübken, F.-J., Hoffman, P., Latteck, R., Baumgarten, G., Blix, T.A., 2003. PMSE dependence on aerosol charge number density and aerosol size. Journal of Geophysical Research 108 (D8), 8441, http://dx.doi.org/10.1029/2002JD002650.

Rapp, M., Lübken, F.-J., 2004. Polar mesosphere summer echoes (PMSE): review of observations and current understanding. Atmospheric Chemistry and Physics 4, 2601–2633.

Rapp, M., Strelnikova, I., Gumbel, J., 2007. Meteoric smoke particles: evidence from rocket and radar techniques. Advances in Space Research 40, 809–817.

Rapp, M., Strelnikova, I., Latteck, R., Hoffman, P., Hoppe, U.-P., Häggström, I., Rietveld, M., 2008. Polar mesospher summer echoes (PMSE) studied at Bragg wavelengths of 28 m, 67 cm, and 16 cm. Journal of Atmospheric and Solar-Terrestrial Physics 70, 947–961, http://dx.doi.org/10.1016/j.jastp.2007.11.005.

Rapp, M., Strelnikova, I., Strelnikov, B., Latteck, R., Baumgarten, G., Li, Q., Megner, L., Gumbel, J., Friedrich, M., Hoppe, U.-P., Robertson, S., 2009. First in situ measurement of the vertical distribution of ice volume in a mesospheric ice cloud during the ECOMA/MASS rocket-campaign. Annales Geophysicae 27, 755–766.

Reid, G.C., 1990. Ice particles and electron "biteout" at the summer polar mesopause. Journal of Geophysical Research 95, 12,896–13,891.

Rietveld, M.T., Kohl, H., Kopka, H., 1993. Introduction to ionospheric heating at Tromsø-1: experimental overview. Journal of Atmospheric and Terrestrial Physics 55, 577–599, http://dx.doi.org/10.1016/0021–9169(93)90007–L.

Röttger, J., LaHoz, C., 1990. Characteristics of polar mesosphere summer echoes (PMSE) observed with the EISCAT 224 MHz radar and possible explanations of their origin. Journal of Atmospheric and Terrestrial Physics 52, 893–906.

Röttger, J., Rietveld, M.T., LaHoz, C., Hall, C., Kelley, M.C., Swartz, W., 1990. Polar mesosphere summer echoes observed with the EISCAT 933-MHz radar and the CUPRI 469 MHz radar their similarity to 224 MHz radar echoes and their relation to turbulence and electron density profiles. Radio Science 25, 671–687.

Singer, W., Latteck, R., Friedrich, M., Wakabayashi, M., Rapp, M., 2011. Seasonal and solar activity variability of D-region electron density at 69 °N. Journal of Atmospheric and Solar-Terrestrial Physics 73, 925–935.

Strelnikova, I., Rapp, M., Raizada, S., Sulzer, M., 2007. Meteor smoke particle properties derived from Arecibo incoherent scatter radar observations. Geophysical Research Letters 34, L15815.

Strelnikova, I., Rapp, M., 2010. Studies of polar mesosphere summer echoes with the EISCAT VHF and UHF radars: information contained in the spectral shape. Advances in Space Research 45, 247–259.

Tanenbaum, B.S., 1968. Continuum theory of Thomson scattering. Physical Review 171, 215–221.

Thomas, G.E., 1991. Mesopheric clouds and the physics of the mesopause region. Reviews of Geophysics 29, 553–575.

Ulwick, J.C., Baker, K.D., Kelley, M.C., Balsley, B.B., Ecklund, W.L., 1988. Comparison of simultaneous MST radar and electron density probe measurements during STATE. Journal of Geophysical Research 93, 6989–7000.

Varney, R.H., Kelley, M.C., Nicolls, M.J., Heinselman, C.J., Collins, R.L., 2011. The electron density dependence of polar mesospheric summer echoes. Journal of Atmospheric and Solar-Terrestrial Physics 73, 2153–2165.

von Zahn, U., Bremer, J., 1999. Simultaneous and common-volume observations of noctilucent clouds and polar mesosphere summer echoes. Geophysical Research Letters 26, 1521–1524.